Numerical simulation of fluid flow and heat transfer inside a rotating disk-cylinder configuration by a lattice Boltzmann model

Sheng Chen,[1,2] Jonas Tölke,[2] and Manfred Krafczyk[2,*]
[1]*State Key Laboratory of Coal Combustion, Huazhong University of Science and Technology, Wuhan 430074, China*
[2]*Institute for Computational Modeling in Civil Engineering, Technical University, Braunschweig 38106, Germany*
(Received 16 March 2009; published 14 July 2009)

A simple lattice Boltzmann model for numerical simulation of fluid flow and heat transfer inside a rotating disk-cylinder configuration, which is of fundamental interest and practical importance in science as well as in engineering, is proposed in this paper. Unlike existing lattice Boltzmann models for such flows, which were based on "primitive-variable" Navier-Stokes equations, the target macroscopic equations of the present model for the flow field are vorticity–stream function equations, inspired by our recent work designed for nonrotating flows [S. Chen, J. Tölke, and M. Krafczyk, Phys. Rev. E **79**, 016704 (2009); S. Chen, J. Tölke, S. Geller, and M. Krafczyk, Phys. Rev. E **78**, 046703 (2008)]. The flow field and the temperature field both are solved by the D2Q5 model. Compared with the previous models, the present model is more efficient, more stable, and much simpler. It was found that, even though with a relatively low grid resolution, the present model can still work well when the Grashof number is very high. The advantages of the present model are validated by numerical experiments.

DOI: 10.1103/PhysRevE.80.016702 PACS number(s): 47.11.−j

I. INTRODUCTION

The complex hydrodynamic behavior of convectional flow inside a coaxial rotating disk-cylinder configuration has for a long time been a subject of considerable attention because of its wide variety of immediate technological applications, for example, Czochralski crystal growth in material engineering [1] and electrodeposition process in electrochemistry [2]. Due to importance of such flows, considerable research efforts, experimental works, as well as analytical and numerical studies have been performed in order to realize their characteristics [3–7]. In the past two decades, particular attentions have been put on the computational fluid dynamics (CFD) studies owing to the complications of such flows [1]. Numerically, the classical CFD methods are based on the direct discretization of the macroscopic governing equations (e.g., the Navier-Stokes equations for flow field and the convection-diffusion equation for temperature field). Generally, the assumption of axisymmetric flow is adopted for simulating such problems. With cylinder coordinates, only one half of the whole domain needs to be computed so the computational cost is significantly reduced [1,3,4]. Although algorithmic advances in CFD methods over the last decade are significant for flows inside a rotating disk-cylinder configuration, the attempt to develop an alternative numerical method for such flows is still continued due to the intrinsic defects of the classical CFD methods in this field [4,8,9].

Recently, the lattice Boltzmann (LB) models have matured for simulating and modeling complicated physical, chemical, and social systems [10–27]. The implementation of a LB procedure is quite easy. Parallelization of a LB model is natural since the relaxation is local and the performance increases nearly linearly with the number of CPUs. Moreover, the LB molds have been compared favorably with spectral methods [28], artificial compressibility methods [29], finite-volume methods [30,31], finite difference methods [32–34], projection methods [35,36], and multigrid method [37], all quantitative results further validate excellent performance of the LB method not only in computational efficiency but also in numerical accuracy. Due to these advantages, the LB method has been successfully used to simulate many problems, from laminar single phase flows to turbulent multiphase flows [12,13].

However, the available open literature on LB models simulating thermal flow inside a coaxial rotating disk cylinder is still quite sparse [4,8,9]. Recently, Bhaumik and Lakshmisha used a three-dimensional D3Q19 multiple-relaxation-time LB model to simulate lid-driven athermal swirling flows in a confined cylindrical cavity [9]. In their work, the fine structures of athermal swirling flows at different aspect ratios (Λ) and Reynolds (Re) numbers were presented. But because the computational demand required for three-dimensional LB models is considerably greater, their discussion was limited in a low regime of Re. Furthermore, since an axisymmetric swirling flow is a quasi-two-dimensional problem for conventional CFD solvers in the cylindrical coordinate system, it obviously decreases the efficiency of the simulation to use a three-dimensional LB model to solve such quasi-two-dimensional problems [4,8]. The difficulty results from that the standard LB model is based on the Cartesian coordinate system and has the essential restriction on the lattice uniformity since all the lattice models are defined on the Cartesian coordinates and the standard LB model will recover the macroscopic equations in the Cartesian coordinate system by Chapman-Enskog expansion [8].

To improve the performance of LB models for such flows, Peng and his copartners extended Halliday's idea [38], which designed for axisymmetric athermal flow without swirl, to simulate thermal flow inside a coaxial rotating disk cylinder

*kraft@irmb.tu-bs.de

[8]. The spirit of Halliday's model is [38]: through the coordinate transformation, the Navier-Stokes equations in the cylindrical coordinate system can be transformed to the specific pseudo-Cartesian representations with "geometrical forcing" terms and then to design a so-called "axisymmetric" LB model to simulate such specific pseudo-Cartesian representations. The outstanding advantage of Halliday's model is that one can use two-dimensional lattice models, such as the D2Q9 model, to simulate quasi-three-dimensional axisymmetric flows. Comparing with three-dimensional LB models, Halliday's model significantly decreases the computational demand required for such flows [9]. But at the same time, it suffers from the puzzle of serious numerical instability. The first and main reason for numerical instability of Halliday's model is that this type of scheme is built on primitive-variables-based governing equations. However, it is well known that for rotating axisymmetric flows primitive-variables-based governing equations are not the best option from the view point of numerical stability and usually vorticity-stream-function equations are chosen alternatively [1]. The second reason for numerical instability is that there are too many quite complex differential expressions in the source terms of Halliday-type LB models although there have been many efforts on trying to reduce this intrinsic negative effect [4,39,40]. Take the model proposed by Peng *et al.*, for example, which is a hybrid scheme, namely, to solve the axial and radial velocity components by the Halliday-type axisymmetric LB model and to solve the azimuthal velocity and the temperature by the central difference scheme [8]. The authors used the hybrid scheme to simulate the Wheeler benchmark problem for Czochralski crystal growth, which is an important generic problem investigated both experimentally and computationally [1,8]. However, because hampered by the numerical instability of Halliday-type model, their discussion is limited in a very narrow range $10^2 \leq \mathrm{Re} \leq 10^3$ and $\mathrm{Gr} \leq 10^5$. It was found that the hybrid LB scheme proposed by Peng *et al.* is unstable for simulations of axisymmetric flows with high Reynolds number ($\mathrm{Re}=10^4$) and high Grashof number ($\mathrm{Gr}=10^6$) even with very fine grid such as 200×200. Furthermore, to guarantee the numerical stability of Peng's model for rotating flows with $\mathrm{Gr}=10^7$, the grid size must be 1000×1000 [4]. However, the Grashof number in most practical cases is more than 10^7 [1], consequently this scheme is hardly used for practical simulations due to its extreme huge demand for computational resources. Later, Huang *et al.* [4] proposed a modified version of Peng's model for axisymmetric swirling and rotating thermal flows. In Huang's model, the incompressible D2Q9 model proposed by He and Luo is used instead of the standard D2Q9 model to improve the numerical stability. In their work, the influence of geometrical forcing terms, which caused by the coordinate transformation, on numerical stability and computational efficiency was discussed in detail and the numerical results were compared with those obtained by the quadratic upstream interpolation for convective kinematics (QUICK) scheme with a grid resolution 80×80. Although Huang's hybrid LB scheme [4] is more numerically stable than Peng's, through numerical tests it was found that for Huang's scheme the grid resolution still has to be improved to 150×150 when $\mathrm{Gr}=10^6$ and at least to 474×474 when $\mathrm{Gr}=10^7$ for numerical stability, which also means the huge demand for computational resources and makes the improved hybrid LB scheme too expensive to simulate practical cases yet.

In order to overcome the above disadvantages, in this paper we propose a simple lattice Boltzmann model to simulate thermal flow inside a coaxial rotating disk cylinder, which is inspired by our recent work designed for axisymmetric nonrotating flows [41,42]. There are two main differences between the present model and the existing LB model for such flows: first, for flow field, the target macroscopic equations of the present model are vorticity-stream-function equations instead of the primitive-variables-based Navier-Stokes equations. As mentioned above, it is the main reason corresponding to numerical instability of Halliday-type model. Second, in the present scheme, the flow field and the temperature field both are solved by the two-dimensional D2Q5 lattice model. The first characteristic makes the present model more stable and more efficient. In the present model, the source terms caused by the coordinate transformation are simpler than that of all existing axisymmetric LB models [4,8,38–40], without any complex terms due to vorticity-stream-function equations instead of Navier-Stokes equations being invoked. Generally speaking, adding complex position and time-dependent source terms into LB models would decrease the numerical stability besides computational efficiency [4]. More important, from the point of numerical analysis, vorticity-stream-function-based equations themselves are more suitable and more efficient than primitive-variables-based ones for axisymmetric swirling and rotating flows, especially for the cases with high Re and high Gr [1]. The second characteristic makes the present model keep the simplicity of code, which is an attractive advantage for both practitioners and novices. In this paper, the present model is validated by numerical experiments. Comparing with the existing hybrid LB schemes [4,8], the present model can still work well when $\mathrm{Gr}=10^7$ with a relative low grid resolution 100×100. Hence, our numerical method provides a significant advantage for simulating convectional flow inside a coaxial rotating disk cylinder with high Reynolds number and high Grashof number. In addition, we have compared the computational efficiency of the vorticity-stream-function-based LB model with that of the traditional LB model and conventional numerical methods. The comparison results show that the vorticity-stream-function-based LB model is the most efficient one[35].

The rest of the paper is organized as follows. The governing equations for thermal flows inside a coaxial rotating disk cylinder are presented in Sec. II. In Sec. III, a simple vorticity-stream-function-based LB model for such flows is introduced. In Sec. IV, numerical experiments are performed to test some properties of the present model. Summary and conclusion are presented in Sec. V.

II. GOVERNING EQUATIONS

The configuration of thermal flows inside a coaxial rotating disk cylinder is illustrated in Fig. 1, same as that in Refs. [1,3–8]. It consists of a vertical cylinder of radius R_c filled

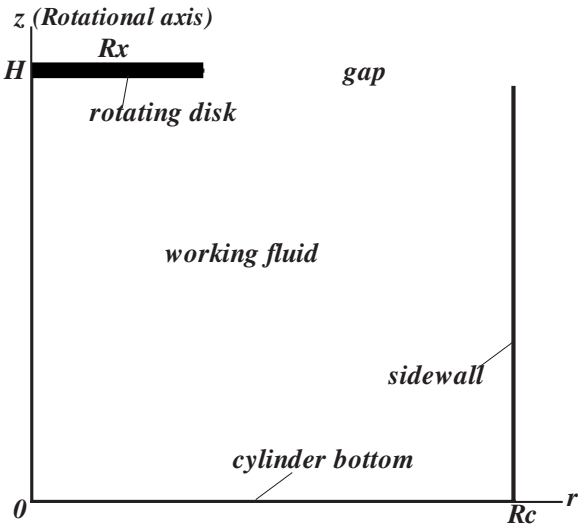

FIG. 1. The configuration of coaxial rotating disk-cylinder.

with working fluid to a height H and rotating with an angular velocity Ω_c. The work fluid is bounded above by a coaxial disk of radius $R_x < R_c$ rotating with angular velocity Ω_x.

The primitive-variable-based formulas of the governing equations in the cylindrical coordinate system can be written as [4,8]

$$\frac{1}{r}\frac{\partial(ru)}{\partial r} + \frac{\partial w}{\partial z} = 0, \tag{1}$$

$$\frac{\partial u}{\partial t} + u\frac{\partial u}{\partial r} + w\frac{\partial u}{\partial z} - \frac{v^2}{r} = -\frac{1}{\rho}\frac{\partial p}{\partial r} + \nu\left(\nabla^2 u - \frac{u}{r^2}\right), \tag{2}$$

$$\frac{\partial v}{\partial t} + u\frac{\partial v}{\partial r} + w\frac{\partial v}{\partial z} + \frac{uv}{r} = \nu\left(\nabla^2 v - \frac{v}{r^2}\right), \tag{3}$$

$$\frac{\partial w}{\partial t} + u\frac{\partial w}{\partial r} + w\frac{\partial w}{\partial z} = -\frac{1}{\rho}\frac{\partial p}{\partial z} + \nu\nabla^2 w + g\alpha(T - T_c), \tag{4}$$

$$\frac{\partial T}{\partial t} + u\frac{\partial T}{\partial r} + w\frac{\partial T}{\partial z} = \kappa\nabla^2 T, \tag{5}$$

where

$$\nabla^2 = \frac{1}{r}\frac{\partial}{\partial r}\left(r\frac{\partial}{\partial r}\right) + \frac{\partial^2}{\partial z^2},$$

u, v, and w are radial, azimuthal, and axial velocity components, p is the pressure, T is the temperature, ν is the kinetic viscosity, g is the gravitational acceleration along the negative z axis, κ is the thermal conductivity, ρ is the density of working fluid, and α is the coefficient of thermal expansion. The subscripts c and x stand for the sidewall and the disk.

Because the coupling term uv/r in the discretized governing equation leads to a false production of angular momentum that is difficult to eliminate, usually a physically conserved quantity the swirl $\Phi = rv$, viz the angular momentum per unit mass, is introduced to overcome this difficulty. Then Eqs. (2) and (3) become [1]

$$\frac{\partial u}{\partial t} + u\frac{\partial u}{\partial r} + w\frac{\partial u}{\partial z} - \frac{\Phi^2}{r^3} = -\frac{1}{\rho}\frac{\partial p}{\partial r} + \nu\left(\nabla^2 u - \frac{u}{r^2}\right), \tag{6}$$

$$\frac{\partial \Phi}{\partial t} + u\frac{\partial \Phi}{\partial r} + w\frac{\partial \Phi}{\partial z} = \frac{\nu}{r}\frac{\partial}{\partial r}\left[r^3\frac{\partial}{\partial r}\left(\frac{\Phi}{r^2}\right)\right] + \nu\frac{\partial^2 \Phi}{\partial z^2}. \tag{7}$$

However, in most practical simulations the more frugal vorticity-stream-function methods are employed instead of the primitive equations [1,41,42]. Because for rotationally symmetric flow, computation time can be reduced if the problem is reformulated so that the three variables u, v, and p are eliminated in favor of the vorticity ω and Stokes stream function ψ, which are defined as [1]

$$\omega = \frac{\partial w}{\partial r} - \frac{\partial u}{\partial z}, \tag{8}$$

$$u = \frac{1}{r}\frac{\partial \psi}{\partial z}, \tag{9}$$

$$w = -\frac{1}{r}\frac{\partial \psi}{\partial r}. \tag{10}$$

The dimensionless vorticity-stream-function-based governing equations read as [1]

$$\frac{\partial S}{\partial t} + u\frac{\partial S}{\partial r} + w\frac{\partial S}{\partial z} + \frac{\partial}{\partial z}\left(\frac{\Phi^2}{r^4}\right) = \frac{\mathrm{Gr}}{\Lambda_R^3 \mathrm{Re}_x^2}\frac{1}{r}\frac{\partial T}{\partial r} + \frac{1}{\mathrm{Re}_x}\left\{\frac{1}{r}\frac{\partial}{\partial r}\left[\frac{1}{r}\frac{\partial}{\partial r}(r^2 S)\right] + \frac{\partial^2 S}{\partial z^2}\right\}, \tag{11}$$

$$\frac{\partial \Phi}{\partial t} + u\frac{\partial \Phi}{\partial r} + w\frac{\partial \Phi}{\partial z} = \frac{1}{\mathrm{Re}_x}\left\{\frac{1}{r}\frac{\partial}{\partial r}\left[r^3\frac{\partial}{\partial r}\left(\frac{\Phi}{r^2}\right)\right] + \frac{\partial^2 \Phi}{\partial z^2}\right\} \tag{12}$$

$$\frac{\partial T}{\partial t} + u\frac{\partial T}{\partial r} + w\frac{\partial T}{\partial z} = \frac{1}{\mathrm{Re}_x \mathrm{Pr}}\left[\frac{1}{r}\frac{\partial}{\partial r}\left(r\frac{\partial T}{\partial r}\right) + \frac{\partial^2 T}{\partial z^2}\right], \tag{13}$$

$$\frac{\partial}{\partial r}\left(\frac{1}{r}\frac{\partial \psi}{\partial r}\right) + \frac{1}{r}\frac{\partial^2 \psi}{\partial z^2} = -rS. \tag{14}$$

In the above equations the vorticity ω is replaced by the Svanberg vorticity $S = \omega/r$ for numerically stable modeling of physically unstable flows [1]. Other independent scaling parameters are the following:

(1) Aspect ratio $\Lambda = H/R_c$.

(2) Ratio of cylinder radius to disk radius $\Lambda_R = R_c/R_x$.

(3) Ratio of cylinder rotation rate to disk rotation rate $\Lambda_\Omega = \Omega_c/\Omega_x$, Ω corresponding to the rotating angular velocity.

(4) Prandtl number $\mathrm{Pr} = \nu/\kappa$.

(5) Reynolds numbers $\mathrm{Re}_c = R_c^2\Omega_c/\nu$ and $\mathrm{Re}_x = R_c^2\Omega_x/\nu$.

(6) Grashof number $\mathrm{Gr} = \alpha g R_c^3 (T_c - T_x)/\nu^2$.

(7) Dimensionless temperature $\bar{T} = (T - T_x)/(T_c - T_x)$ for simplification the overline is omitted in the rest part.

III. COORDINATE TRANSFORMATION AND CORRESPONDING LATTICE BOLTZMANN MODEL

By performing the following coordinate transformation [4,8]:

$$(r,z) \mapsto (x,y), \tag{15}$$

$$(u,w) \mapsto (u,v). \tag{16}$$

Equations (9)–(14) can be written in the pseudo-Cartesian coordinates:

$$u = \frac{1}{x}\frac{\partial \psi}{\partial y}, \tag{17}$$

$$v = -\frac{1}{x}\frac{\partial \psi}{\partial x}, \tag{18}$$

$$\frac{\partial S}{\partial t} + u\frac{\partial S}{\partial x} + v\frac{\partial S}{\partial y} = \frac{1}{\mathrm{Re}_x}\left(\frac{\partial^2 S}{\partial x^2} + \frac{\partial^2 S}{\partial y^2}\right) + S_o, \tag{19}$$

$$\frac{\partial \Phi}{\partial t} + u\frac{\partial \Phi}{\partial x} + v\frac{\partial \Phi}{\partial y} = \frac{1}{\mathrm{Re}_x}\left(\frac{\partial^2 \Phi}{\partial x^2} + \frac{\partial^2 \Phi}{\partial y^2}\right) + \Phi_o, \tag{20}$$

$$\frac{\partial T}{\partial t} + u\frac{\partial T}{\partial x} + v\frac{\partial T}{\partial y} = \frac{1}{\mathrm{Re}_x\,\mathrm{Pr}}\left(\frac{\partial^2 T}{\partial x^2} + \frac{\partial^2 T}{\partial y^2}\right) + T_o, \tag{21}$$

$$\frac{\partial^2 \psi}{\partial y^2} + \frac{\partial^2 \psi}{\partial x^2} = \Theta. \tag{22}$$

In Eqs. (19)–(22), the source terms caused by the coordinate transformation read as

$$S_o = \frac{3}{x\,\mathrm{Re}_x}\frac{\partial S}{\partial x} + \frac{\mathrm{Gr}}{\Lambda_R^3\,\mathrm{Re}_x^2}\frac{1}{x}\frac{\partial T}{\partial x} - \frac{2\Phi}{x^4}\frac{\partial \Phi}{\partial y}, \tag{23}$$

$$\Phi_o = -\frac{1}{x\,\mathrm{Re}_x}\frac{\partial \Phi}{\partial x}, \tag{24}$$

$$T_o = \frac{1}{x\,\mathrm{Re}_x\,\mathrm{Pr}}\frac{\partial T}{\partial x}, \tag{25}$$

$$\Theta = -(r^2 S + v). \tag{26}$$

Bearing in mind that from now on u and v stand for the velocity components along x and y coordinates.

Equations (19)–(21), which have the same formulation except different coefficients, are nothing but advection-diffusion equations with source terms. There are many matured efficient lattice Boltzmann models for this type of equation [17,43–47]. In this paper the D2Q5 model proposed in our previous work [41,42] is employed. It reads as

$$g_k(\vec{x} + c\vec{e}_k\Delta t, t + \Delta t) - g_k(\vec{x},t) = -\tau^{-1}[g_k(\vec{x},t) - g_k^{(eq)}(\vec{x},t)] + \Delta t \Upsilon_{o,k}, \tag{27}$$

where $\vec{e}_k (k=0,\ldots,4)$ are the discrete velocity directions:

$$\vec{e}_k = \begin{cases} (0,0) & k=0 \\ (\cos(k-1)\pi/2,\ \sin(k-1)\pi/2) & k=1,2,3,4. \end{cases}$$

$c=\Delta x/\Delta t$ is the fluid particle speed. Δx, Δt and τ are the lattice grid spacing, the time step, and the dimensionless relaxation time, respectively. $\Upsilon_{o,k}$ is the first-order term of the expansion of the source term Υ_o [17,44], $\Upsilon_o = S_o, \Phi_o, T_o$ for Eqs. (19)–(21), respectively. $\Upsilon_{o,k}$ satisfies

$$\sum_{k\geq 0} \Upsilon_{o,k} = \Upsilon_o. \tag{28}$$

In this paper we simply choose

$$\Upsilon_{o,k} = \frac{\Upsilon_o}{5}. \tag{29}$$

Compared with the existing LB models for axisymmetric swirling and rotating flows [4,8], the expression of $\Upsilon_{o,k}$ in the present model is the simplest one without any complex term.

The equilibrium distribution $g_k^{(eq)}$ is defined by

$$g_k^{(eq)} = \frac{\delta}{5}\left[1 + 2.5\frac{\vec{e}_k \cdot \vec{u}}{c}\right], \tag{30}$$

where $\delta = S, \Phi, T$ for Eqs. (19)–(21), respectively, and is obtained by

$$\delta = \sum_{k\geq 0} g_k, \tag{31}$$

and the dimensionless relaxation time τ is determined by

$$\chi = \frac{5}{2c^2(\tau - 0.5)}, \tag{32}$$

where $\chi = \mathrm{Re}_x, \mathrm{Re}_x, \mathrm{Re}_x\,\mathrm{Pr}$ for Eqs. (19)–(21), respectively.

Equation (22) is just the Poisson equation, which also can be solved by the LB method [47–54] or the multigrid method [55,56]. In the present paper, the D2Q5 model used in our previous work [41,42] is employed to solve the Poisson equation. The evolution equation for Eq. (22) reads as

$$f_k(\vec{x} + c\vec{e}_k\Delta t, t + \Delta t) - f_k(\vec{x},t) = \Omega_k + \Omega_k', \tag{33}$$

where $\Omega_k = -\tau_\psi^{-1}[f_k(\vec{x},t) - f_k^{(eq)}(\vec{x},t)]$, $\Omega_k' = \Delta t \zeta_k \Theta D$, and $D = \frac{c^2}{2}(0.5 - \tau_\psi)$. $\tau_\psi > 0.5$ is the dimensionless relaxation time [48]. $f_k^{(eq)}$ is the equilibrium distribution function and defined by

$$f_k^{(eq)} = \begin{cases} (\xi_0 - 1.0)\psi & k=0 \\ \xi_k \psi & k=1,2,3,4, \end{cases}$$

where ξ_k and ζ_k are weight parameters given as $\xi_0 = \zeta_0 = 0$, and $\xi_k = \zeta_k = 1/4 (k=1,\ldots,4)$. ψ is defined by

$$\psi = \sum_{k\geq 1} f_k. \tag{34}$$

Through the Chapman-Enskog expansion, Eqs. (19)–(22) can be recovered straightforwardly from Eqs. (27) and (33), which is very similar with the process presented in Ref. [42].

The multigrid method perhaps is a better alternative for solving Poisson equation and the present authors have devel-

TABLE I. Some results for the test cases by the present model, the hybrid LB schemes [4,8] and QUICK [57]. (a) Present work; (b) Ref. [4]; (c) Ref. [57]; (d) Ref. [8].

Case	Gr	Re_x	Re_c	$\psi_{min}^{(a)}$	$\psi_{max}^{(a)}$	$\psi_{min}^{(b)}$	$\psi_{max}^{(b)}$	$\psi_{min}^{(c)}$	$\psi_{max}^{(c)}$	$\psi_{min}^{(d)}$	$\psi_{max}^{(d)}$
*A*1	0	10^2	0	-2.381×10^{-1}	7.891×10^{-6}	-2.272×10^{-1}	7.921×10^{-6}	-2.172×10^{-1}	4.063×10^{-6}	-2.210×10^{-1}	5.460×10^{-6}
*A*2	0	10^3	0	-3.286×10^{0}	7.403×10^{-5}	-4.979×10^{0}	7.311×10^{-5}	-4.994×10^{0}	1.826×10^{-5}	-5.075×10^{0}	1.060×10^{-4}
*A*3(256)	0	10^4	0	-4.188×10^{1}	2.497×10^{-1}	-4.047×10^{1}	2.413×10^{-1}	-4.117×10^{1}	1.044×10^{-1}		
*B*1	0	10^2	−25	-3.582×10^{-2}	1.109×10^{-1}	-4.785×10^{-2}	1.140×10^{-1}	-4.433×10^{-2}	1.177×10^{-1}	-5.140×10^{-2}	1.440×10^{-1}
*B*2	0	10^3	−250	-1.272×10^{0}	1.103×10^{0}	-1.491×10^{0}	1.084×10^{0}	-1.478×10^{0}	1.148×10^{0}	-1.478×10^{0}	1.114×10^{0}
*B*3(256)	0	10^4	−2500	-8.473×10^{0}	5.227×10^{0}	-8.226×10^{0}	5.075×10^{0}	-8.725×10^{0}	5.388×10^{0}		
*C*1	10^5	0	0	-2.337×10^{-3}	2.835×10^{1}	-1.213×10^{-3}	2.863×10^{1}	-5.798×10^{-4}	2.841×10^{1}	-5.180×10^{-3}	2.988×10^{1}
*C*2	10^6	0	0	-2.715×10^{-1}	9.270×10^{1}	-3.805×10^{-1}	9.320×10^{1}	-1.200×10^{-1}	9.251×10^{1}		
*C*3	10^7	0	0	-5.104×10^{0}	2.001×10^{2}			-2.240×10^{0}	1.850×10^{2}		
*D*1	10^5	10^1	0	-7.810×10^{-4}	2.815×10^{1}	-1.178×10^{-3}	2.863×10^{1}	-5.785×10^{-4}	2.841×10^{1}		
*D*2	10^5	10^2	0	-1.618×10^{-4}	2.837×10^{1}	-1.564×10^{-4}	2.860×10^{1}	-4.517×10^{-4}	2.838×10^{1}		
*D*3	10^5	10^3	0	-4.284×10^{-1}	2.511×10^{1}	-5.562×10^{-1}	2.528×10^{1}	-5.677×10^{-1}	2.517×10^{1}		

oped a multigrid solver for discrete Boltzmann equation [56]. The attempt using a multigrid-method-based LB solver to solve Eq. (22) is under consideration.

IV. NUMERICAL RESULTS

In the present paper, the boundary conditions are

$$S = -\frac{2}{r^2\Delta z^2}\psi(r,\Lambda_R\Lambda-\Delta z,t), \quad \Omega = r^2, \quad T=-0.5, \quad \psi=0 \tag{35}$$

on the rotating disk,

$$S = -\frac{2}{\Lambda_R^2\Delta r^2}\psi(\Lambda_R-\Delta r,z,t), \quad \Omega = \Lambda_\Omega\Lambda_R^2, \quad T=0.5, \quad \psi=0 \tag{36}$$

on the sidewall,

$$S = -\frac{2}{r^2\Delta r}\psi(r,\Delta z,t), \quad \Omega = \Lambda_\Omega r^2, \quad \frac{\partial T}{\partial z}=0, \quad \psi=0 \tag{37}$$

on the cylinder bottom,

$$S=0, \quad \frac{\partial\Omega}{\partial z}=0, \quad T=T_x+\frac{r-R_x}{R_c-R_x}(T_c-T_x), \quad \psi=0 \tag{38}$$

on the gap, and the axisymmetric boundary condition [8] for the rotational axis $r=0$. Δz and Δr are grid distances in axial and radial directions, respectively. The boundary conditions used in the present paper are same as that in Refs. [4,8,57].

To validate the present model, as many as 12 cases of convectional flows inside a coaxial rotating disk cylinder with difference parameter sets were simulated. The 12 cases were classified into four groups. In group A, the disk rotates with Re_x varying from 10^2 to 10^4, while the cylinder is at rest and Gr is set to zero. In group B, the disk and cylinder rotate in opposite directions. Groups A and B are all forced convection problems. Cases in group C are natural convection problems with $10^5 \le Gr \le 10^7$. Cases in group D are more like practical applications because these flows combined both the natural convection and forced convection were investigated.

In our simulations, Pr=0.05, Λ_R=2.5, Λ_Ω=0.4, and Λ=1, same as those in Refs. [4,8,57]. In order to get grid-independent numerical results, in this paper we employed several different grid resolutions, from 80×80 to 256×256, and found that the grid resolution 100×100 is sufficient to obtain accurate results for most cases except when $Re_x=10^4$.

Table I lists the comparison of computed minimum and maximum stream functions for all the above 12 cases. In the table, the number in the bracket followed the case type indicates the grid size used. If not specified, the grid used in our simulation is 100×100. For comparison, we also present the results of Xu *et al.* [57] using the second-order difference scheme with a grid resolution 80×80 and those in Refs.

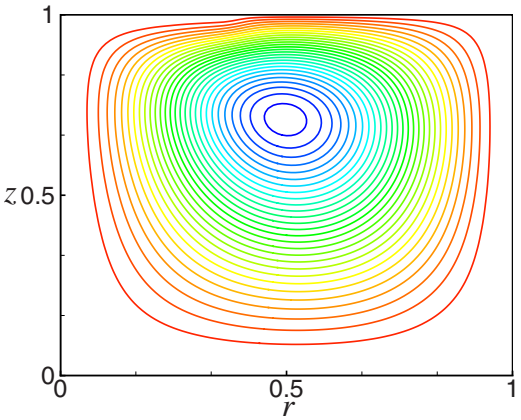

FIG. 2. (Color online) Streamlines of case $A2$: Gr=0, $\mathrm{Re}_x=10^3$, $\mathrm{Re}_c=0$.

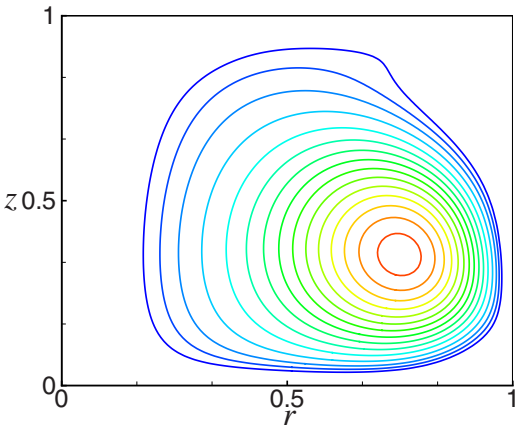

FIG. 4. (Color online) Streamlines of case $C2$: $\mathrm{Gr}=10^6$, $\mathrm{Re}_x=0$, $\mathrm{Re}_c=0$.

[4,8] obtained by hybrid LB schemes for axisymmetric swirling and rotating flows. In all cases, the maximum absolute values of stream function computed by the present model agree very well with the previous data [4,8,57]. Some very small deviations between the computed minimum absolute values of stream function can be neglected since the minimum absolute values of stream function are so small compared with the maximum absolute values. It was found that the hybrid LB scheme proposed by Peng *et al.* [8] was unstable for simulations of melt flows with high Reynolds number and high Grashof number even with very fine grid (for example, grid size 1000×1000 for $\mathrm{Gr}=10^7$) [4]. Although Huang's hybrid LB scheme [4] is more numerically stable than Peng's, the grid resolution still has to be improved to 150×150 when $\mathrm{Gr}=10^6$ and at least to 474×474 when $\mathrm{Gr}=10^7$ for numerical stability, which means the huge demand for computational resources and makes the hybrid LB scheme too expensive to simulate practical flows since most practical melt flows with $\mathrm{Gr}\geq10^7$. Comparing to the existing hybrid LB schemes [4,8], the present model can still work well when $\mathrm{Gr}=10^7$ with a relative low grid resolution 100×100. Hence, our numerical method provides a significant advantage for simulating thermal flows inside a coaxial rotating disk cylinder with high Reynolds number and high Grashof number since vorticity-stream-function equations instead of Navier-Stokes equations are invoked in the preset model.

Figure 2 shows the calculated streamlines of case A2, which typifies the calculations of group A. In this group, it can be observed that when the disk rotation speed is increased while the cylinder is at rest, the absolute value of the stream function increases, which means that the intensity of vortex increases, and the center of the vortex induced by the rotation moves toward the sidewall of the cylinder and is deformed increasingly. Meanwhile, the highest velocity region moves from the upper left corner to the upper right corner, while the lowest velocity region is enlarged in the lower left corner.

Figure 3 gives the streamlines of case $B2$, which represents the flow pattern of group B. For cases in group B, the disk and cylinder rotate in opposite directions. As a result, there are two vortices with opposite directions appearing in the upper left corner just below the disk and the lower right corner. With the increase in rotation speeds of the disk and cylinder, the upper left vortex produced by the disk rotation moves toward right corner, whereas the lower right vortex induced by the cylinder rotation moves to left and dominates the flow field.

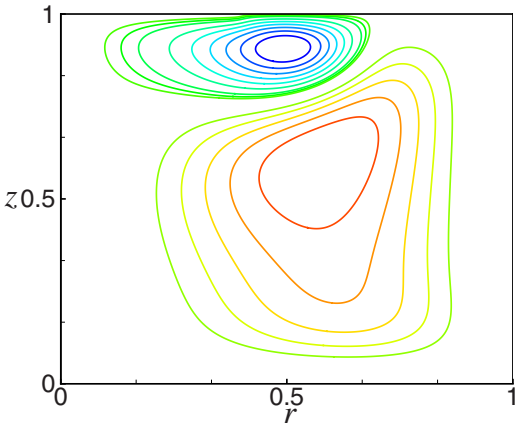

FIG. 3. (Color online) Streamlines of case $B2$: Gr=0, $\mathrm{Re}_x=10^3$, $\mathrm{Re}_c=-250$.

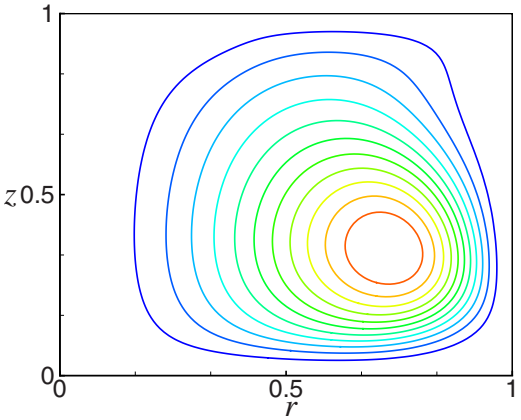

FIG. 5. (Color online) Streamlines of case $D2$: $\mathrm{Gr}=10^5$, $\mathrm{Re}_x=10^2$, $\mathrm{Re}_c=0$.

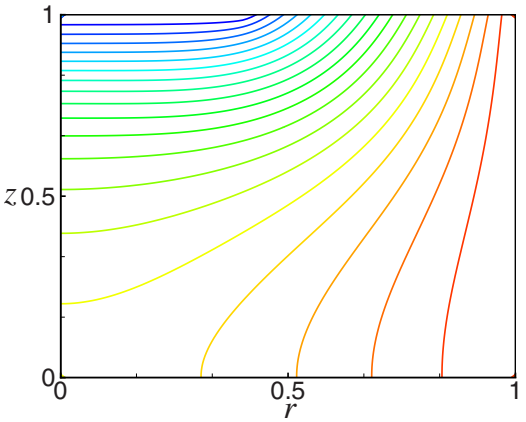

FIG. 6. (Color online) Temperature contours of case $A1$: Gr=0, $\mathrm{Re}_x=10^2$, $\mathrm{Re}_c=0$.

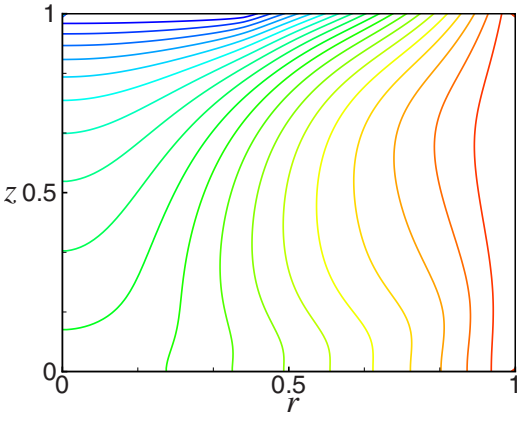

FIG. 8. (Color online) Temperature contours of case $C1$: Gr $=10^5$, $\mathrm{Re}_x=0$, $\mathrm{Re}_c=0$.

Figure 4 depicts the streamlines of case $C2$, typifying the calculations belonging to group C. In this group, the disk and cylinder are at rest and the sidewall Grashof number increases from 10^5 to 10^7. When Gr increases, the vortex gets enlarged and its highest velocity layer moves to the sidewall of the cylinder. It should be noted that the center of vortex seems not to change its position at all.

Figure 5 describes the streamlines of case $D2$, which serve as a representation for group D. The streamlines illustrated the combined effects of the natural convective flow and forced convective flow. It is found that the streamlines of cases in group D are very similar to those of case $C1$ whose Grashof number is also equal to 10^5. From Table I, it is also found that the ψ_{max} of cases in group D are all very close to that of case $C1$. That means in cases of group D, if $\mathrm{Re}_x < 10^3$, the natural convective flow dominates the flow while the force convective flow induced by the disk only has minor effect.

Figures 6–9 illustrate the temperature contours of cases $A1$, $B1$, $C1$, and $D2$, which represent the contours of temperature of corresponding groups. Case $D2$ is a combination of case $A1$ and $C1$. From Figs. 6 and 7, it is very clear that for cases of forced convection problems where Gr=0 (cases in group A and B), the contours of temperature are very similar. On the contrary, the temperature field for the Case $C1$, namely Fig. 8, is quite different from cases $A1$ and $B1$, and this shows the effect of buoyancy force on the temperature field. Figure 9 is very similar with Fig. 8, which means in cases of group D, if $\mathrm{Re}_x < 10^3$, the natural convective flow dominates the flow while the force convective flow induced by the disk only has minor effect, agreeing well with the conclusion draw from the flow pattern, viz Fig. 5.

V. CONCLUSION

In this paper we proposed a simple lattice Boltzmann model for convectional flows inside a coaxial rotating disk cylinder. Unlike previous axisymmetric LB models, which based on primitive-variable Navier-Stokes equations, the target macroscopic equations of the present model for flow field are vorticity-stream-function equations. Benefitting from the intrinsic features of vorticity-stream-function equations, the geometrical forcing term due to the coordinate transformation needs to be expanded just to first order in the present model and the constraint on its discrete form is very simple, without any complex term. Moreover, both the flow field and the temperature field are simulated by the two-dimensional

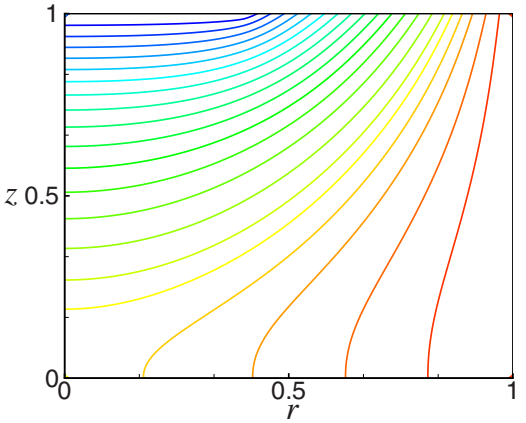

FIG. 7. (Color online) Temperature contours of case $B1$: Gr=0, $\mathrm{Re}_x=10^2$, $\mathrm{Re}_c=-25$.

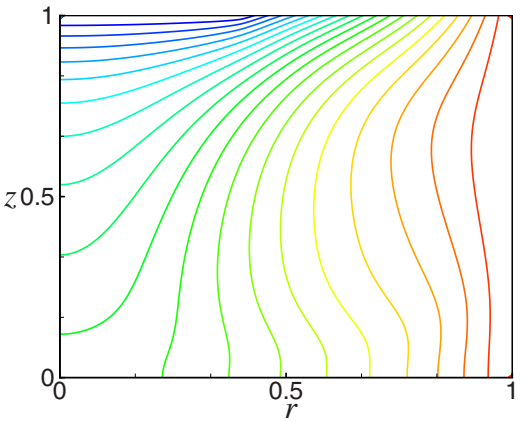

FIG. 9. (Color online) Temperature contours of case $D2$: Gr $=10^5$, $\mathrm{Re}_x=10^2$, $\mathrm{Re}_c=0$.

D2Q5 lattice model. Therefore the present model is more efficient, more stable and much simpler than the existing models.

We validated the present model by simulating thermal flows inside a coaxial rotating disk cylinder with $\mathrm{Re}_x \leq 10^4$ and $\mathrm{Gr} \leq 10^7$, which is investigated both experimentally and computationally. The fine structures of flow patterns and temperature distributions are described clearly by the present model. The numerical results agree well with previous studies. Comparing with the existing hybrid LB schemes, even with a low grid resolution, the present model can still work well when Gr is very high. Consequently, our numerical method provides a significant advantage for simulating thermal flows inside a coaxial rotating disk cylinder.

ACKNOWLEDGMENTS

This work was partially supported by the Alexander von Humboldt Foundation, Germany. One of the authors (S.C.) would like to thank Professor B. C. Shi, Department of Mathematics, Huazhong University of Science and Technology, China, for his helpful discussions during this work. The present authors would like to gratefully acknowledge the referees for their valuable advice and comments.

[1] W. E. Langlois, Annu. Rev. Fluid Mech. **17**, 191 (1985).
[2] Ph. Mandin, C. Fabian, and D. Lincot, Electrochim. Acta **51**, 4067 (2006).
[3] T. Inamuro, A. Yamaguchi, F. Ogino, Heat Transfer, Asian Res. **28**, 172 (1999).
[4] H. Huang, T. S. Lee, and C. Shu, Int. J. Numer. Methods Fluids **53**, 1707 (2007).
[5] Y. Khine and J. Walker, J. Cryst. Growth **165**, 372 (1996).
[6] C. Lee and J. Hyun, Int. J. Heat Fluid Flow **20**, 26 (1999).
[7] X. Ruiz, M. Aguilo, J. Massons, and F. Diaz, Exp. Fluids **14**, 333 (1993).
[8] Y. Peng, C. Shu, Y. T. Chew, and J. Qiu, J. Comput. Phys. **186**, 295 (2003).
[9] S. K. Bhaumik and K. N. Lakshmisha, Comput. Fluids **36**, 1163 (2007).
[10] Y. Qian, D. d'Humieres, and P. Lallemand, Europhys. Lett. **17**, 479 (1992).
[11] R. Benzi, S. Succi, and M. Vergassola, Phys. Rep. **222**, 145 (1992).
[12] S. Chen and G. D. Doolen, Annu. Rev. Fluid Mech. **30**, 329 (1998).
[13] S. Succi, *The Lattice Boltzmann Equation for Fluid Dynamics and Beyond* (Oxford University Press, Oxford, 2001).
[14] S. Chen, Z. Liu, Z. He, C. Zhang *et al.*, Int. J. Mod. Phys. C **18**, 187 (2007).
[15] S. Chen, M. Krafczyk, Int. J. Therm. Sci. (to be published).
[16] A. J. C. Ladd, J. Fluid Mech. **271**, 311 (1994).
[17] S. P. Dawson, S. Chen, G. D. Doolen, D. R. Janecky, and A. Lawniczak, Comput. Chem. Eng. **19**, 617 (1995).
[18] Y. H. Qian, S. Succi, and S. Orszag, in Annual Reviews of Computational Physics, Vol. 3, edited by D. Stauffer (World Scientific, Singapore, 1995), pp. 195–242.
[19] G. Hazi, A. R. Imre, G. Mayer *et al.*, Ann. Nucl. Energy **29**, 1421 (2002).
[20] D. Yu, R. Mei, L. S. Luo *et al.*, Prog. Aerosp. Sci. **39**, 329 (2003).
[21] M. C. Sukop and D. T. Thorne, Jr., *Lattice Boltzmann Modeling: An Introduction for Geoscientists and Engineers* (Springer, Heidelberg, Berlin, 2006).
[22] S. Arcidiacono, J. Mantzaras, and I. V. Karlin, Phys. Rev. E **78**, 046711 (2008).
[23] D. Qi, J. Chem. Phys. **125**, 114901 (2006).
[24] C. Sun, C. Migliorini, and L. Munn, Biophys. J. **85**, 208 (2003).
[25] S. Chen, Z. Liu, B. Shi *et al.*, Appl. Math. Comput. **173**, 33 (2006).
[26] D. Raabe, Modell. Simul. Mater. Sci. Eng. **12**, R13 (2004).
[27] J. Meng, Y. Qian, X. Li, and S. Dai, Phys. Rev. E **77**, 036108 (2008).
[28] D. O. Martinez, W. H. Matthaeus, S. Chen *et al.*, Phys. Fluids **6**, 1285 (1994).
[29] X. He, G. D. Doolen, and T. Clark, J. Comput. Phys. **179**, 439 (2002).
[30] Y. Y. Al-Jahmany, G. Brenner, and P. O. Brunn, Int. J. Numer. Methods Fluids **46**, 903 (2004).
[31] A. Al-Zoubi and G. Brenner, Int. J. Mod. Phys. C **15**, 307 (2004).
[32] T. Seta, E. Takegoshi, and K. Okui, Math. Comput. Simul. **72**, 195 (2006).
[33] S. Chen, B. Shi, Z. Liu, Z. He, Z. Guo, and C. Zheng, Chin. Phys. **13**, 1657 (2004).
[34] S. Chen, Z. Liu, B. Shi, Z. He, and C. Zheng, Acta Mech. Sin. **21**, 574 (2005).
[35] S. Chen, J. Tolke, and M. Krafczyk, Comput. Methods Appl. Mech. Eng. **198**, 367 (2008).
[36] S. Chen, Appl. Math. Comput. (to be published).
[37] S. Chen, B. Shi, Z. Liu, Z. He *et al.*, Chin. Phys. Lett. **23**, 656 (2006).
[38] I. Halliday, L. A. Hammond, C. M. Care, K. Good, and A. Stevens, Phys. Rev. E **64**, 011208 (2001).
[39] T. Reis and T. N. Phillips, Phys. Rev. E **75**, 056703 (2007).
[40] T. Reis, T. N. Phillips, Phys. Rev. E **77**, 026703 (2008).
[41] S. Chen, J. Tolke, S. Geller, and M. Krafczyk, Phys. Rev. E **78**, 046703 (2008).
[42] S. Chen, J. Tolke, and M. Krafczyk, Phys. Rev. E **79**, 016704 (2009).
[43] B. Deng, B. Shi, and G. Wang, Chin. Phys. Lett. **22**, 267 (2005).
[44] S. Chen, Z. Liu, C. Zhang *et al.*, Appl. Math. Comput. **193**, 266 (2007).
[45] H. J. Liu, C. Zou, B. C. Shi *et al.*, Int. J. Heat Mass Transfer **49**, 4672 (2006).
[46] Z. L. Guo, B. C. Shi, and C. G. Zheng, Int. J. Numer. Methods Fluids **39**, 325 (2002).
[47] I. Ginzburg, Adv. Water Resour. **28**, 1171 (2005).
[48] Z. Chai and B. Shi, Appl. Math. Model. **32**, 2050 (2008).

[49] I. Ginzburg, Adv. Water Resour. **28**, 1196 (2005).
[50] X. He and N. Ling, Comput. Phys. Commun. **129**, 158 (2000).
[51] Z. Guo, T. S. Zhao, and Y. Shi, J. Chem. Phys. **122**, 144907 (2005).
[52] Z. Chai, Z. Guo, B. Shi, J. Appl. Phys. **101**, 104913 (2007).
[53] J. Wang, M. Wang, and Z. Li, J. Colloid Interface Sci. **296**, 729 (2006).
[54] M. Hirabayashi, Y. Chen, and H. Ohashi, JSME Int. J., Ser. B **44**, 45 (2001).
[55] S. Melchionna and S. Succi, J. Chem. Phys. **120**, 4492 (2004).
[56] J. Tolke, M. Krafczyk, and E. Rank, J. Stat. Phys. **107**, 573 (2002).
[57] D. Xu, C. Shu, and B. C. Khoo, J. Cryst. Growth **173**, 123 (1997).